MethodsX 11 (2023) 102409

Contents lists available at ScienceDirect

MethodsX

journal homepage: www.elsevier.com/locate/methodsx

Liquid phase exfoliation of $MoSe_2$: Effect of solvent on morphology, edge confinement, bandgap and number of layers study

Honey Mittal, Maryam Raza, Manika Khanuja*

Centre for Nanoscience and Nanotechnology, Jamia Millia Islamia, New Delhi 110025, India

ARTICLE INFO

Method name:
Liquid Phase Exfoliation

Keywords:
Liquid phase exfoliation
$MoSe_2$
2D materials
Optical properties

ABSTRACT

In this study, a facile and scalable method for synthesizing $MoSe_2$ nanomaterial via a sonication-assisted liquid-phase exfoliation method is proposed. This study shows the successful synthesis of few-layered $MoSe_2$ in various solvents including DI water, ethanol, N-Methyl-2-pyrrolidone (NMP), Dimethylformamide (DMF) and Dimethylsulfoxide (DMSO). The exfoliated nanosheets have remarkably different properties than bulk $MoSe_2$ which were studied using Field emission scanning electron microscopy, Fourier-transform infrared spectroscopy, X-ray diffraction and UV–Vis spectroscopy to investigate their morphology, functional groups, structure and optical properties, respectively. The mean values of the number of layers from an optical extinction spectrum based on the effect of edge and quantum confinement were also calculated. Moreover, the exfoliated material using this method has potential application in energy storage as demonstrated by the electrochemical performance of the bulk and exfoliated materials.

- Successful synthesis of the few-layer $MoSe_2$ from bulk $MoSe_2$ using liquid phase exfoliation method in various solvents
- The investigation of the effect of solvent on the number of layers and optical properties of $MoSe_2$

Specification Table

Subject area:	Material Science
More specific subject area:	2D materials
Name of your method:	Liquid Phase Exfoliation
Name and reference of the original method:	N.A.
Resource availability:	Tip sonicator from electronics industries at 200 V

Introduction

2D materials have become the subject of research due to their enormous properties and diversified applications [1–4]. 2D materials exhibit remarkable changes in the mechanical, chemical and physical characteristics when the thickness is reduced down to the atomic level layer extent [5]. At present, there is a diverse range of 2D layered materials that can be isolated from their bulk counterparts such as black phosphorus, graphene, MoS_2, $MoSe_2$, MnO_2, etc. [6,7] Molybdenum diselenide ($MoSe_2$) is a layered 2D semiconductor

* Corresponding author.
E-mail address: mkhanuja@jmi.ac.in (M. Khanuja).

https://doi.org/10.1016/j.mex.2023.102409
Received 3 February 2023; Accepted 27 September 2023
Available online 28 September 2023
2215-0161/© 2023 The Author(s). Published by Elsevier B.V. This is an open access article under the CC BY-NC-ND license (http://creativecommons.org/licenses/by-nc-nd/4.0/)

Table 1
2D materials produced via sonication as a function of exfoliation time and solvent.

Material	Sonication Time (hour)	Morphology	Solvent	Ref.
MoS_2	1	Nanosheets	CHP, DMA, DMF	[5]
WS_2	1	Nanosheets	DMA, DMF, DMSO	
BN	1	Nanosheets	Methanol, DMA, Acetone	
MoS_2	12	Nanosheets	DMF, NMP, Formamide	[8]
Graphite	1	Nanosheets	HFB, TFB, PFBN and PFP	[27]
MoS_2	3.5	Quantum dots	NMP	[28]
Black Phosphorus	4	Nanosheets	ACN	[29]
MoS_2	–	Nanosheets	NMP	[30]
Black Phosphorus	24	phosphorene nanosheets	NMP	[31]
Bulk $MoSe_2$	20	Nanosheets	Lysine	[32]
Graphene Nanosheets		Nanoflakes	NMP, GBL, DMEU and DMA	[33]
Black Phosphorus	15	Nanoflakes	DMF, DMSO	[34]
$MoSe_2$	2.5	Nanosheets	NMP	[35]
Graphene	4	Nanosheets	SC	
WS_2	2.5	Nanosheets	CHP	

*DMF: Dimethylformamide, NMP: N-Methyl pyrrolidone, ACN: Acetonitrile, GBL: Gamma-butyrolactone, DMEU: Dimethyl ethylene urea, DMA: Dimethylacetamide, DMSO: Dimethyl sulfoxide, HFB: Hexafluorobenzene, TFB: Trifluorobenzene, PFP: Pentafluoropyridine, PFBN: Pentaflorobenzonitrile, SC: Sodium Cholate, CHP: N–Cyclohexyl-2-pyrrolidone.

material that belongs to the transition metal dichalcogenides (TMDs) [8–11]. $MoSe_2$ possesses good chemical stability, high surface area and catalytic activity making it a potential candidate to be used in various applications including lubricants, photocatalysts, energy storage, electrocatalysis and biosensors [12–15].

Exfoliation is the latest approach to achieve high-quality 2D materials, which includes liquid-phase exfoliation and mechanical exfoliation [16,17]. Mechanical exfoliation was mainly applied for the production of single-layer or few-layered 2D materials from their bulk counterparts. Mechanical exfoliation is a pollution-free method, however, it is not suitable for large-scale production due to the lack of repeatability [15,16]. Liquid phase exfoliation has a lot of advantages including solution processing capability, stability, low cost and the ability to produce high-quality sheets [15]. Liquid phase exfoliation is a multipurpose method for generating liquid suspensions by sonication or shearing of layered materials in liquids and producing defect-free nanosheets. The efficient exfoliation and stable dispersion require the match of the surface tension of the solvent with the material [18]. The series of solvents with surface tension between 40 and 50 mJm^{-2} can efficiently exfoliate $MoSe_2$ by reducing the interfacial tension between $MoSe_2$ and the solvent [9]. Numerous studies have reported the correlation between solvent surface tension and exfoliation efficiency. Ng et al. reported the liquid phase exfoliation of graphene using green solvent and selected the solvent by matching the surface tension of graphite and the solvent [19,20]. Morton et al. published the liquid phase exfoliation of graphite using eco-friendly solvent and also optimized the ultrasonication conditions and achieved better quality flakes with improved stability [21,22]. Kaur et al. studied the effect of temperature and acoustic pressure on the sono-exfoliation of graphene using water as a solvent [7]. Qin et al. developed a simulation model for bubble oscillation and collapse dynamics under sonication. The mechanisms of particle dispersion in relation to surface properties of materials and bubble oscillation dynamics were also proposed. A relationship model was also established to understand the connection between produced shock waves and forces on the material surface [23,24]. Tyurnina et al. produced few-layer graphene up to 3 layers via liquid phase exfoliation using two ultrasound sources of different frequencies. The optimization of the frequency and pressure of the ultrasonic source resulted in the highest concentration of flakes. The relationship between the thickness, surface area and yield of graphene as well as with the frequency and intensity of an ultrasonic source is also established [25,26]. The examples of 2D materials produced via sonication are summarized in Table 1.

In this study, the liquid phase exfoliation of $MoSe_2$ in different solvents including DI Water, ethanol, NMP, DMF and DMSO has been investigated. There are confined numbers of reports that correlate the number of layers with solvent. The effect of solvent on the texture coefficient and optical properties of the bulk and exfoliated $MoSe_2$ was studied using XRD diffractogram and UV–Vis spectroscopy, respectively. The exfoliated nanosheets showed a reduced number of layers as compared to the bulk material. In addition, the electrochemical performance was also tested and exfoliated materials exhibited superior electrochemical performance as compared with the bulk $MoSe_2$.

Materials

Bulk $MoSe_2$ (99.9 %) was purchased from Aldrich, and ethanol (C_2H_5OH) with 99.9 % purity was supplied by Merck. N-Methyl-2-Pyrrolidone (NMP) ($CH_2(CH_2)_2CONCH_3$) with 99.5 % purity and N,Ndimethylformamide (DMF) ($HCON(CH_3)_2$) with 99 % purity was purchased from Thermo Fisher Scientific India Pvt. Ltd and Merck Specialties Private Limited, respectively. Dimethylsulphoxide (DMSO) ($(CH_3)_2SO$) with a purity of 99.5 % was supplied by Avantor Performance Materials India Limited.

Synthesis

A Liquid-phase exfoliation is a straightforward and most suitable method for large-scale production. The liquid phase exfoliation mechanism is shown in Fig. 1. The suitable solvent for the exfoliation of layered materials is determined by its ability to closely match

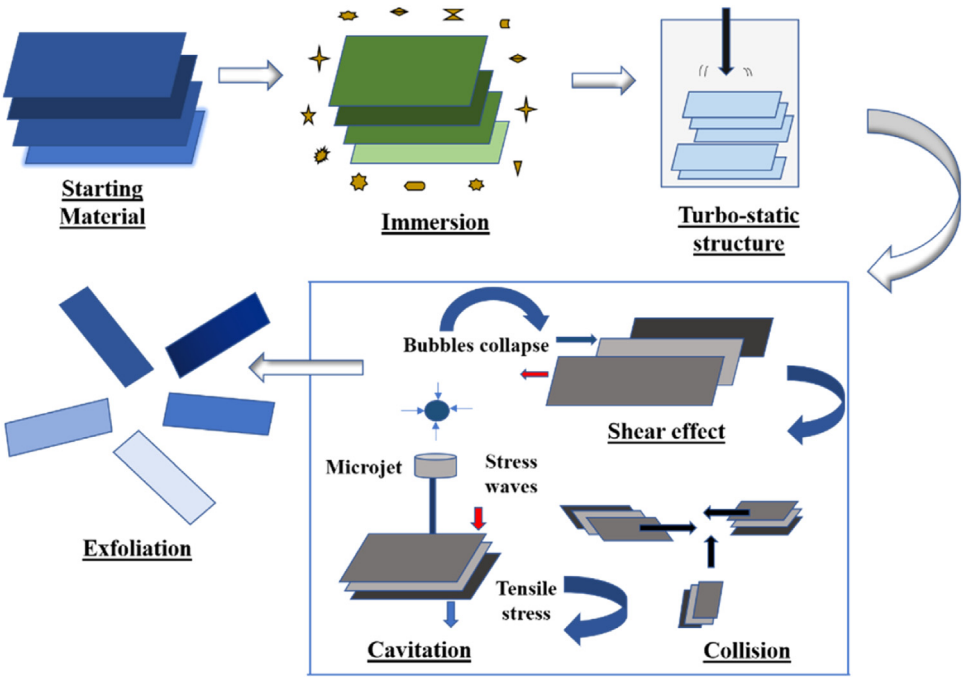

Fig. 1. Possible mechanism for exfoliation of bulk $MoSe_2$.

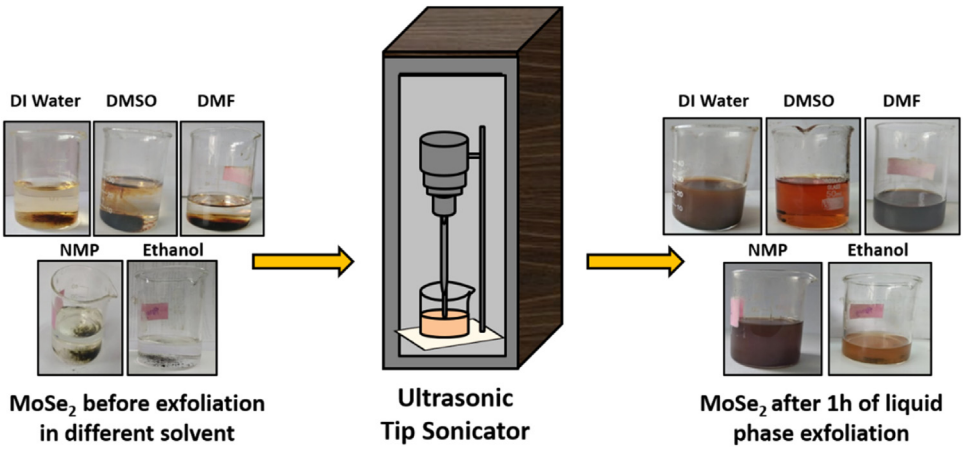

Fig. 2. Schematic of liquid phase exfoliation technique (Left: $MoSe_2$ completely settles down at the bottom of solvent and Right: Solubilization of $MoSe_2$ in respective solvents gives a dark colloidal dispersion).

the surface tension of the layered material. Energy is introduced into the system through sonication to surpass the van der Waals cohesive forces acting among the layers of the bulk nanomaterial. The separation of individual layers begins when there is enough energy to overcome the binding energy. Microcavities are created by the high-frequency vibration (>15 kHz) of the probe which collapses and causes a high-energy pulse to emanate and shear the layered nanomaterial [33]. The shear forces originating from the burst of cavitation bubbles facilitate the exfoliation of layers within the material [36]. The selection of a suitable solvent is of prime importance as the suitable solvent not only improves the exfoliation but also sustains stable dispersions at high concentrations [37].

The liquid phase exfoliation of highly dispersed suspension of $MoSe_2$ in different solvents was performed using an ultrasonic probe sonicator as shown in Fig. 2. The surface tension of DI water, ethanol, NMP, DMF and DMSO is 72.00, 22.10, 40.79, 37.10 and 43.54 N/m, respectively [9,38,39]. 40 mg of $MoSe_2$ powder was added to 40 mL of solvent in a beaker and sonicated in an ultrasonic probe sonicator for 1 h. 1 mL of solution was extracted after a fixed interval of 10 min to measure the optical transmission using a UV–Visible spectrophotometer.

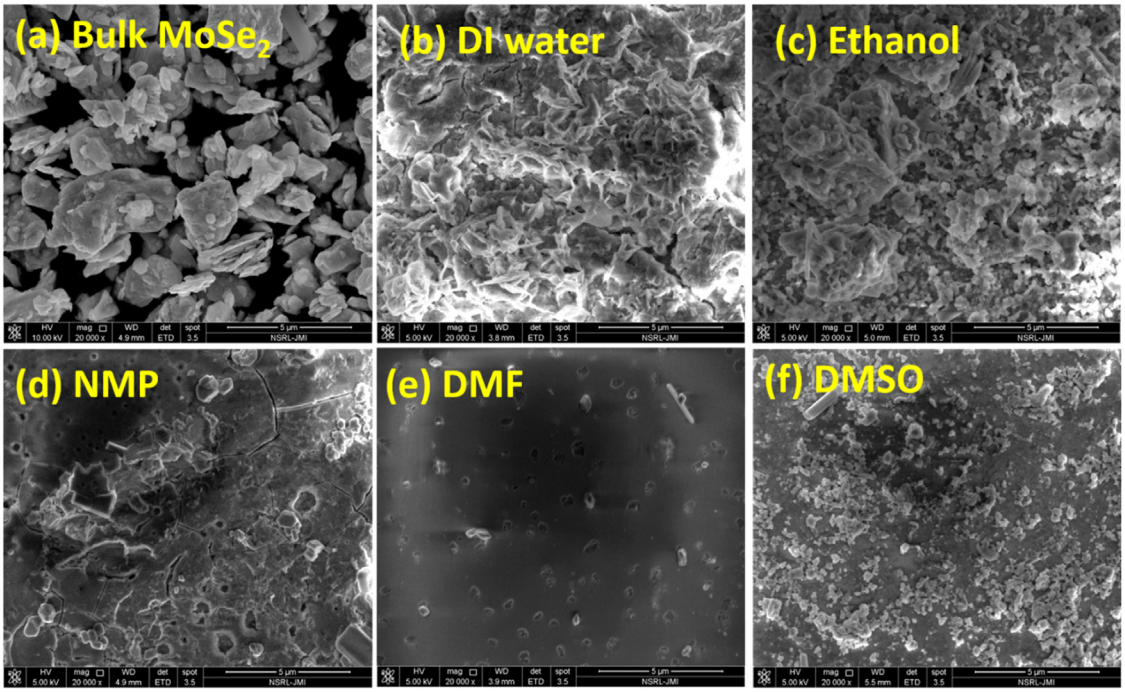

Fig. 3. FESEM images of the (a) bulk $MoSe_2$ and liquid phase exfoliated $MoSe_2$ using (b) DI water, (c) ethanol, (d) NMP, (e) DMF and (f) DMSO solvent.

Characterizations

The morphology of the materials was examined by FESEM from Quanta 3D FEG. The crystallinity and texture coefficient of the material were investigated using XRD from Rigaku Smart Lab. The Cu K_α radiation with a wavelength of 1.540 Å was used to study the XRD diffractogram in the range of 2θ: 5–70°. UV–Vis spectrophotometer from Agilent Technologies, model-Cary 100 series was used to study the optical properties of the materials. The baseline subtraction for the UV–Vis spectra of exfoliated $MoSe_2$ was done using the respective solvent. FTIR spectroscopy from Bruker Tensor 37 spectrometer was used to analyze the vibrational bands of the material in the range of 400–4000 cm^{-1}. The electrochemical characterizations were performed using three electrode system from the Metrohm autolab workstation. The active material deposited on platinum was used as the working electrode, while Ag/AgCl and platinum wire were used as the reference and counter electrode, respectively.

Results and discussions

Fig. 3 shows the FESEM images of the bulk $MoSe_2$ and $MoSe_2$ nanosheets exfoliated using a liquid-phase exfoliation process utilizing various solvents. As shown in Fig. 3(a), the bulk $MoSe_2$ nanosheets were agglomerated and size distribution was uneven. Fig. 3(b) showed $MoSe_2$ nanosheets after being exfoliated using DI water, the nanosheets were noticed to be crippled into small sheets after the exfoliation. Fig. 3(c) showed the $MoSe_2$ nanosheets exfoliated using ethanol, it was observed that the nanosheets remained largely intact, without significant breakage or surface damage. Fig. 3(d–f) showed $MoSe_2$ nanosheets exfoliated using NMP, DMF and DMSO, respectively. The aggregates were broken down, particle size was reduced, particles were uniformly dispersed and the agglomeration between nanosheets was avoided effectively.

The crystalline structures of bulk $MoSe_2$ and as-exfoliated $MoSe_2$ nanosheets were characterized using XRD as shown in Fig. 4(i). The presence of several peaks in the XRD diffractogram of bulk $MoSe_2$ confirms the presence of numerous layers. The bulk $MoSe_2$ powder exhibited peaks positioned at 2θ: 13.6°, 27.5°, 31.4°, 37.9°, 41.9°, 47.5°, 55.8° and 56.8° corresponded to (002), (004), (100), (103), (006), (105), (110) and (008), respectively as shown in Fig. 4i(a) (JCPDS no. 29–0914). The exfoliated $MoSe_2$ nanosheets showed dominant orientation towards the (002) plane, and some distinguished peaks that were present in the bulk $MoSe_2$ were absent in the exfoliated $MoSe_2$ which is in agreement with previously reported reports [40]. These results confirm that the few-layered $MoSe_2$ has been successfully synthesized.

The other structural parameter, texture coefficient was calculated from the XRD data to investigate the relative transition intensities before and after the exfoliation. The equilibrium between energy dissipation and the incoming flux holds great significance in the development of texture due to the involvement of kinetic and thermodynamic processes in texture advancement [41]. The texture coefficient of the plane denotes the orientation pattern of a particular crystallographic plane. The deviation from the orientation found in the basic bulk sample suggests favorable growth conditions. The rate of $TC_{(002)}$ declines as the number of layers or average

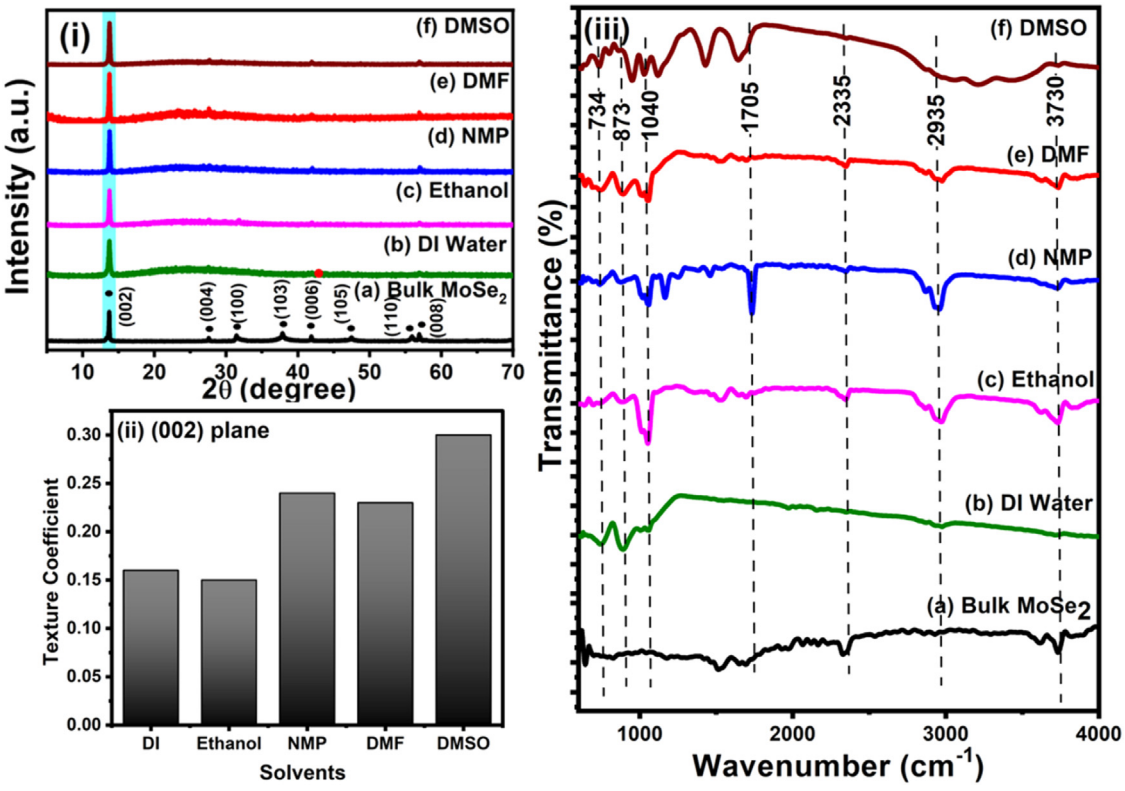

Fig. 4. (i) XRD diffractograms, (ii) Texture coefficient and (iii) FTIR spectra of bulk $MoSe_2$ powder and the liquid phase exfoliated $MoSe_2$ using DI Water, ethanol, NMP, DMF and DMSO solvent.

crystalline size increases. The texture coefficient ($TC_{(hkl)}$) of the (002) plane is determined from the XRD diffractogram using the following formula:

$$TC_{(hkl)} = \sum \frac{1}{N} \left[\frac{I_{(hkl)}}{I_{0(hkl)}} \right] \quad \text{(i)}$$

The texture coefficient for the diffraction peak in different solvents of the exfoliated sample was calculated from their intensities relative to each other as per equation (i), in which $TC_{(hkl)}$ is the texture coefficient, I_{hkl} is the intensity of the peak in the exfoliated sample, $I_{0(hkl)}$ is the intensity of the peak in the bulk sample and N is the number of considered peaks [42]. The calculated texture coefficients of $MoSe_2$ with various solvents are as shown in Fig. 4(ii). The calculated texture coefficient values for $MoSe_2$ exfoliated using DI water, ethanol, NMP, DMF and DMSO are 0.16, 0.15, 0.24, 0.23 and 0.30, respectively. The texture coefficient values show that DMSO exhibited the maximum TC followed by NMP and DMF.

To study the bonding and interaction between $MoSe_2$ and solvent, FTIR spectroscopy was carried out. The FTIR spectra of bulk $MoSe_2$ and $MoSe_2$ exfoliated in DI water, ethanol, NMP, DMF and DMSO are as shown in Fig. 4iii(a-f), respectively. As observed from the FTIR spectrum, the exfoliated $MoSe_2$ spectra showed distinctive peaks and spectral modifications as compared to bulk $MoSe_2$. The characteristic vibrational peaks were present in both bulk and exfoliated $MoSe_2$ spectra. The peaks at 2935 cm^{-1} and 2852 cm^{-1} corresponded to C–H vibrations and the CH_2 groups [43]. The peak at 2335 cm^{-1} corresponded to the C–O stretching mode [44]. The peak located at 1705 cm^{-1} is attributed to the C=O stretching and COO^- bonds [45]. The band corresponding to the Se-O stretching vibration was observed at 1040 cm^{-1}, confirming the successful production of $MoSe_2$ [46]. The peak positioned at 873 cm^{-1} may be due to the structural damage of $MoSe_2$ nanosheets in the solution and the peak at 741 cm^{-1} is related to the Mo-O bond [47]. The FTIR spectra confirm the alterations in the vibrational modes of the exfoliated $MoSe_2$.

The UV–Vis absorption spectra of $MoSe_2$ at regular intervals of 10 min during sonication were studied to understand the ability of the solvent to disperse the $MoSe_2$ [48]. Fig. 5(a–e) shows the absorbance spectra of $MoSe_2$ exfoliated using DI water, ethanol, NMP, DMF and DMSO solvent in the wavelength range of 600–900 nm. The excitonic peaks in the range of 695 and 800 nm confirm the successful dispersion of bulk $MoSe_2$ in the solvents. It can be concluded from the observed results that the DMSO showed the best dispersing ability because it exhibits the highest absorption intensity followed by the NMP and DMF. The higher absorbance intensity in optical absorption implies a higher yield of exfoliated $MoSe_2$ nanosheets.

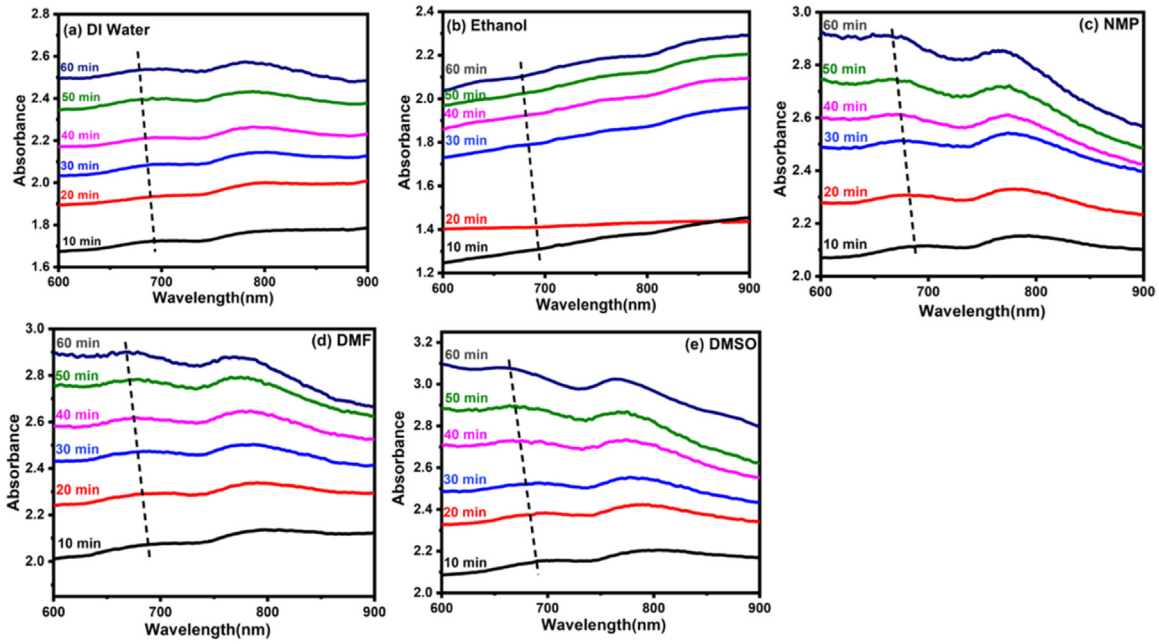

Fig. 5. UV–Vis absorption spectra of liquid phase exfoliated $MoSe_2$ using (a) DI Water, (b) ethanol, (c) NMP, (d) DMF and (e) DMSO solvent.

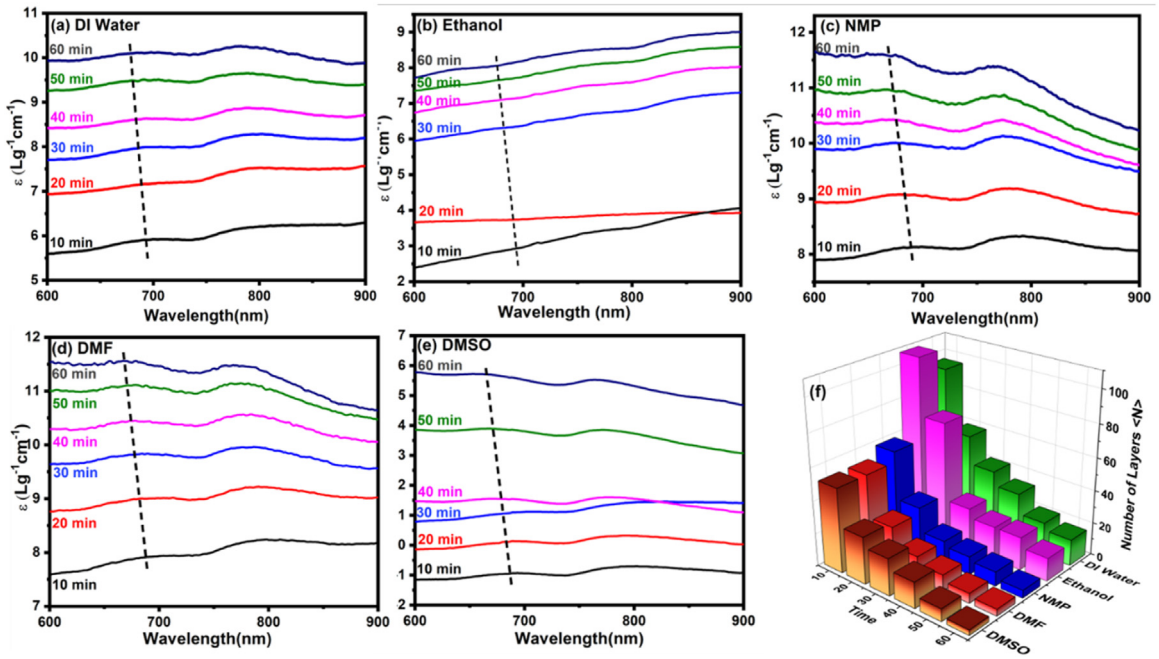

Fig. 6. Extinction spectra of liquid exfoliated $MoSe_2$ in (a) DI Water, (b) ethanol, (c) NMP, (d) DMF and (e) DMSO solvent and (f) exfoliation time vs average number of layers for different solvents.

Fig. 6(a–e) shows optical extinction spectra of exfoliated $MoSe_2$ in different solvents. The extinction coefficient (ε) can be calculated using the following equations:

$$T = 10^{-Ext} \tag{ii}$$

$$E_{xt} = \varepsilon C l \tag{iii}$$

Where T is the transmission, ε is the extinction coefficient, C is the concentration of material and l is the cuvette thickness [49]. Optical extinction spectra of exfoliated transition metal dichalcogenides show characteristic excitonic peaks that vary systematically

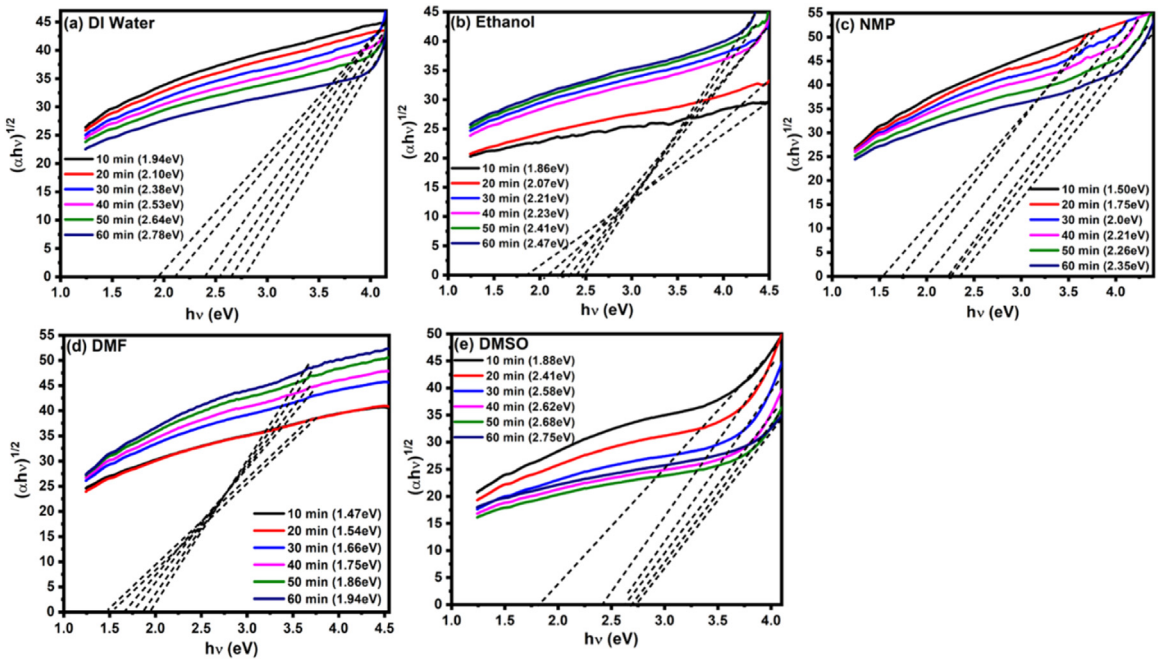

Fig. 7. Tauc's plot of liquid exfoliated $MoSe_2$ in (a) DI Water, (b) ethanol, (c) NMP, (d) DMF and (e) DMSO solvent.

with exfoliation time. The A and B extinction peaks of $MoSe_2$ are positioned in the range of 695 and 800 nm, respectively [50]. The peak in the range of 695 nm is attributed to the direct excitonic transition at the K-point in the Brillouin zone [51,52]. The spectra depend on the length and mean nanosheet thickness of $MoSe_2$ nanosheets due to effect of edge and confinement effect, respectively [53,54]. The A-exciton peak exhibit blue shift in wavelength with exfoliation time is due to the reduction in number of layers of the nanosheets. The average number of layers of $MoSe_2$ nanosheets can be calculated using equation (iv):

$$\langle N \rangle = 2.3 \times 10^{36} e^{-54{,}888/\lambda} \quad \text{(iv)}$$

Where N is the layer number and λ is the excitonic peak position [6,55]. Fig. 6(f) shows a comparative average number of layers with the exfoliated time for different solvents. The average layer number of $MoSe_2$ was 95, 108, 58, 52 and 51 for DI water, ethanol, NMP, DMF and DMSO, respectively in the first 10 min. The average layer number of bulk $MoSe_2$ decreased to 15, 14, 5, 4 and 3 for DI water, ethanol, NMP, DMF and DMSO, respectively in 60 min. DMSO, NMP and DMF acted as a successful solvent and decreased the average number of layers significantly in 60 min.

The band gap of the nanomaterial is larger than the bulk counterpart of that material. The indirect bandgap increases with reducing the number of layers of the material whereas the direct band gap remains nearly constant [56]. The bandgap of the exfoliated $MoSe_2$ was calculated using tauc's plot to further investigate the impact of solvents. The tauc's plot of $MoSe_2$ exfoliated using DI water, ethanol, NMP, DMF and DMSO is as shown in Fig. 7(a–e). Band gap energies were estimated from the plot of $(\alpha h\upsilon)^{1/2}$ vs $h\upsilon$, where α is absorption coefficient, characterized as $a = 2.303$ A/t, where "A" is absorbance and t is the thickness of cuvette. Liquid phase exfoliation of $MoSe_2$ in various solvents revealed that band gap of the increases with exfoliated time. Band gap increases from 1.94 to 2.78 eV for DI water, from 1.86 to 2.47 eV for ethanol, from 1.50 to 2.35 eV for NMP, from 1.47 to 1.94 eV for DMF and from 1.88 to 2.75 eV for DMSO. The exfoliated $MoSe_2$ shows broad range of bandgap which has significant potential for technological applications and could be particularly intriguing in the advancement of TMD heterostructures [57].

Electrochemical performance

The electrochemical performance of the exfoliated $MoSe_2$ was tested in three electrode system using 1 M Na_2SO_4 as electrolyte. The Fig. 8(a) shows the cyclic voltammetry (CV) curve at a scan rate of 100 mVs^{-1} within a potential window of 0 to 0.5 V for bulk and exfoliated $MoSe_2$ using different solvents. The exfoliated $MoSe_2$ shows similar redox peaks with the higher surface area corresponding to the larger specific capacitance as compared to bulk $MoSe_2$. The $MoSe_2$ exfoliated in DMSO shows highest specific capacitance followed by NMP and DMF. The electrochemical impedance spectroscopy (EIS) of bulk and exfoliated $MoSe_2$ using different solvents is shown in Fig. 8(b). The Nyquist plot is semicircular with interfacial charge transfer resistance (R_{ct}) of 1.07, 0.97, 0.90, 0.55, 0.51 and 0.39 kΩ for bulk and exfoliated $MoSe_2$ using ethanol, DI water, DMF, NMP and DMSO, respectively. These results confirm the fast oxidation and better charge transfer kinetics in exfoliated $MoSe_2$ as compared to bulk $MoSe_2$.

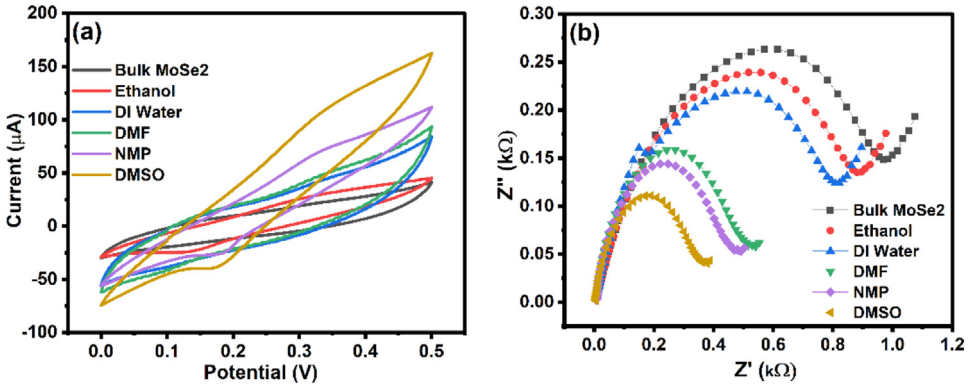

Fig. 8. (a) Cyclic Voltammetry and (b) electrochemical impedance spectroscopy of bulk $MoSe_2$ and $MoSe_2$ exfoliated using different solvent.

Conclusion

The bulk $MoSe_2$ was exfoliated by the facile and low-cost liquid phase exfoliation process by utilizing various solvents. This study identified suitable organic solvents (NMP, DMF and DMSO) in which $MoSe_2$ nanosheets can be exfoliated with high dispersion and long-term stability. The exfoliated $MoSe_2$ nanosheets exhibit the reduced number of layers as supported by XRD diffractograms and extinction spectra. Finally, the electrochemical performance of exfoliated $MoSe_2$ nanosheets exhibited enhanced charge transfer and fast oxidation as compared to bulk $MoSe_2$ indicating it as a potential candidate for energy storage applications. The ease of synthesizing $MoSe_2$ nanosheets with high performance characteristics, this research has the potential to create new avenues for large-scale production of two-dimensional materials.

Ethics statement

This article does not contain any studies involving animals, humans and social media performed by any of the authors.

Data availability

No data was used for the research described in the article.

CRediT authorship contribution statement

Honey Mittal: Conceptualization, Visualization, Data curation, Formal analysis. **Maryam Raza:** Conceptualization, Visualization, Data curation, Formal analysis. **Manika Khanuja:** Writing – original draft, Writing – review & editing.

Acknowledgments

The author is thankful to the Department of Science and Technology, India (DST/NM/NB/2018/203(G)(JMI)) and UGC Start up grant (No.F.4(201-FRP)/2015(BSR)) for their financial support.

Declaration of Competing Interest

The authors declare that they have no known competing financial interests or personal relationships that could have appeared to influence the work reported in this paper.

References

[1] W. Ashraf, A. Khan, S. Bansal, M. Khanuja, Mechanical ball milling: a sustainable route to induce structural transformations in tungsten disulfide for its photocatalytic applications, Phys. E Low Dimens. Syst. Nanostruct. 140 (2022) 115152, doi:10.1016/j.physe.2022.115152.
[2] A. Kumar, H. Mittal, R. Nagar, M. Khanuja, The synergistic effect of acid-etched g-C_3 N_4 nanosheets and polyaniline nanofibers for the adsorption and photocatalytic degradation of textile dyes: a study of charge transfer mechanism and intermediate products, Mater. Adv. 3 (2022) 5325–5336, doi:10.1039/d1ma01218e.
[3] S. Lin, Y. Chui, Y. Li, S.P. Lau, Liquid-phase exfoliation of black phosphorus and its applications, FlatChem 2 (2017) 15–37, doi:10.1016/j.flatc.2017.03.001.
[4] A. Kumar, S. Singh, M. Khanuja, A comparative photocatalytic study of pure and acid-etched template free graphitic C_3N_4 on different dyes: an investigation on the influence of surface modifications, Mater. Chem. Phys. 243 (2020) 122402, doi:10.1016/j.matchemphys.2019.122402.
[5] J.N. Coleman, M. Lotya, A. O'Neill, S.D. Bergin, P.J. King, U. Khan, K. Young, A. Gaucher, S. De, R.J. Smith, I.V. Shvets, S.K. Arora, G. Stanton, H.Y. Kim, K. Lee, G.T. Kim, G.S. Duesberg, T. Hallam, J.J. Boland, J.J. Wang, J.F. Donegan, J.C. Grunlan, G. Moriarty, A. Shmeliov, R.J. Nicholls, J.M. Perkins, E.M. Grieveson, K. Theuwissen, D.W. McComb, P.D. Nellist, V. Nicolosi, Two-dimensional nanosheets produced by liquid exfoliation of layered materials, Science 331 (2011) 568–571, doi:10.1126/science.1194975.

[6] N. Chaudhary, S. Bansal, M. Khanuja, Edge, confinement effects, and measurement of the number of layers of MoS_2 nanosheets by liquid-exfoliated method assisted by different solvents, Int. Nano Lett. 11 (2021) 233–239, doi:10.1007/s40089-021-00337-x.

[7] A. Kaur, J.A. Morton, A.V. Tyurnina, A. Priyadarshi, A. Holland, J. Mi, K. Porfyrakis, D.G. Eskin, I. Tzanakis, Temperature as a key parameter for graphene sono-exfoliation in water, Ultrason. Sonochem. 90 (2022) 106187, doi:10.1016/j.ultsonch.2022.106187.

[8] X. Gan, H. Zhao, K.Y. Wong, D.Y. Lei, Y. Zhang, X. Quan, Covalent functionalization of MoS_2 nanosheets synthesized by liquid phase exfoliation to construct electrochemical sensors for Cd (II) detection, Talanta 182 (2018) 38–48, doi:10.1016/j.talanta.2018.01.059.

[9] G. Cunningham, M. Lotya, C.S. Cucinotta, S. Sanvito, S.D. Bergin, R. Menzel, M.S.P. Shaffer, J.N. Coleman, Solvent exfoliation of transition metal dichalcogenides: dispersibility of exfoliated nanosheets varies only weakly between compounds, ACS Nano 6 (2012) 3468–3480, doi:10.1021/nn300503e.

[10] K.G. Zhou, N.N. Mao, H.X. Wang, Y. Peng, H.L. Zhang, A mixed-solvent strategy for efficient exfoliation of inorganic graphene analogues, Angew. Chem. Int. Ed. 50 (2011) 10839–10842, doi:10.1002/anie.201105364.

[11] H. Mittal, A. Ivaturi, M. Khanuja, $MoSe_2$ modified ZIF-8 novel nanocomposite for photocatalytic remediation of textile dye and antibiotic contaminated wastewater, Environ. Sci. Pollut. Res. 30 (2022) 4151–4165, doi:10.1007/s11356-022-22487-x.

[12] H. Mittal, M. Khanuja, Nanosheets- and nanourchins-like nanostructures of $MoSe_2$ for photocatalytic water purification: kinetics and reusability study, Environ. Sci. Pollut. Res. 27 (2020) 23477–23489, doi:10.1007/s11356-019-06275-8.

[13] I. Siddiqui, H. Mittal, V.K. Kohli, P. Gautam, M. Ali, M. Khanuja, Hydrothermally synthesized micron sized, broom-shaped $MoSe_2$ nanostructures for superior photocatalytic water purification, Mater. Res. Express 5 (2018) 125020.

[14] H. Mittal, A. Kumar, M. Khanuja, $MoSe_2$-PANI nanocomposite as supercapacitor electrode material: optimization, mechanism and electrochemical performance, Chem. Select. 7 (2022) e202201623.

[15] T. Liu, Z. Cui, X. Li, H. Cui, Y. Liu, Al-doped $MoSe_2$ monolayer as a promising biosensor for exhaled breath analysis: a DFT study, ACS Omega 6 (2021) 988–995, doi:10.1021/acsomega.0c05654.

[16] W. Ashraf, A. Khan, S. Bansal, M. Khanuja, Mechanical ball milling : a sustainable route to induce structural transformations in tungsten disulfide for its photocatalytic applications, Phys. E Low Dimens. Syst. Nanostruct. 140 (2022) 115152.

[17] D. Sahoo, B. Kumar, J. Sinha, S. Ghosh, S.S. Roy, B. Kaviraj, Cost effective liquid phase exfoliation of MoS_2 nanosheets and photocatalytic activity for wastewater treatment enforced by visible light, Sci. Rep. 10 (2020) 10759, doi:10.1038/s41598-020-67683-2.

[18] Y. Xu, H. Cao, Y. Xue, B. Li, W. Cai, Liquid-phase exfoliation of graphene: an overview on exfoliation media, techniques, and challenges, Nanomaterials 8 (2018) 942, doi:10.3390/nano8110942.

[19] A.V. Tyurnina, J.A. Morton, A. Kaur, J. Mi, N. Grobert, K. Porfyrakis, I. Tzanakis, D.G. Eskin, Effects of green solvents and surfactants on the characteristics of few-layer graphene produced by dual-frequency ultrasonic liquid phase exfoliation technique, Carbon N. Y. 206 (2023) 7–15, doi:10.1016/j.carbon.2023.01.062.

[20] K.L. Ng, B.M. Maciejewska, L. Qin, C. Johnston, J. Barrio, M.M. Titirici, I. Tzanakis, D.G. Eskin, K. Porfyrakis, J. Mi, N. Grobert, Direct evidence of the exfoliation efficiency and graphene dispersibility of green solvents toward sustainable graphene production, ACS Sustain. Chem. Eng. 11 (2023) 58–66, doi:10.1021/acssuschemeng.2c03594.

[21] J.A. Morton, M. Khavari, L. Qin, B.M. Maciejewska, A.V. Tyurnina, N. Grobert, D.G. Eskin, J. Mi, K. Porfyrakis, P. Prentice, I. Tzanakis, New insights into sono-exfoliation mechanisms of graphite: *in situ* high-speed imaging studies and acoustic measurements, Mater. Today 49 (2021) 10–22, doi:10.1016/j.mattod.2021.05.005.

[22] J.A. Morton, A. Kaur, M. Khavari, A.V. Tyurnina, A. Priyadarshi, D.G. Eskin, J. Mi, K. Porfyrakis, P. Prentice, I. Tzanakis, An eco-friendly solution for liquid phase exfoliation of graphite under optimised ultrasonication conditions, Carbon N. Y. 204 (2023) 434–446, doi:10.1016/j.carbon.2022.12.070.

[23] L. Qin, K. Porfyrakis, I. Tzanakis, N. Grobert, D.G. Eskin, K. Fezzaa, J. Mi, Multiscale interactions of liquid, bubbles and solid phases in ultrasonic fields revealed by multiphysics modelling and ultrafast X-ray imaging, Ultrason. Sonochem. 89 (2022) 106158, doi:10.1016/j.ultsonch.2022.106158.

[24] L. Qin, B.M. Maciejewska, T. Subroto, J.A. Morton, K. Porfyrakis, I. Tzanakis, D.G. Eskin, N. Grobert, K. Fezzaa, J. Mi, Ultrafast synchrotron X-ray imaging and multiphysics modelling of liquid phase fatigue exfoliation of graphite under ultrasound, Carbon N. Y. 186 (2022) 227–237, doi:10.1016/j.carbon.2021.10.014.

[25] A.V. Tyurnina, I. Tzanakis, J. Morton, J. Mi, K. Porfyrakis, B.M. Maciejewska, N. Grobert, D.G. Eskin, Ultrasonic exfoliation of graphene in water: a key parameter study, Carbon N. Y. 168 (2020) 737–747, doi:10.1016/j.carbon.2020.06.029.

[26] A.V. Tyurnina, J.A. Morton, T. Subroto, M. Khavari, B. Maciejewska, J. Mi, N. Grobert, K. Porfyrakis, I. Tzanakis, D.G. Eskin, Environment friendly dual-frequency ultrasonic exfoliation of few-layer graphene, Carbon N. Y. 185 (2021) 536–545, doi:10.1016/j.carbon.2021.09.036.

[27] A.B. Bourlinos, V. Georgakilas, R. Zboril, T.A. Sterioti, A.K. Stubos, Liquid-phase exfoliation of graphite towards solubilized graphenes, Small 5 (2009) 1841–1845, doi:10.1002/smll.200900242.

[28] D. Gopalakrishnan, D. Damien, M.M. Shaijumon, MoS_2 quantum dot-interspersed exfoliated MoS_2 nanosheets, ACS Nano 8 (2014) 5297–5303, doi:10.1021/nn501479e.

[29] Z. Yan, X. He, L. She, J. Sun, R. Jiang, H. Xu, F. Shi, Z. Lei, Z.H. Liu, Solvothermal-assisted liquid-phase exfoliation of large size and high quality black phosphorus, J. Mater. 4 (2018) 129–134, doi:10.1016/j.jmat.2018.01.003.

[30] A. Gupta, V. Arunachalam, S. Vasudevan, Liquid-phase exfoliation of MoS_2 nanosheets: the critical role of trace water, J. Phys. Chem. Lett. 7 (2016) 4884–4890, doi:10.1021/acs.jpclett.6b02405.

[31] J.R. Brent, N. Savjani, E.A. Lewis, S.J. Haigh, D.J. Lewis, P. O'Brien, Production of few-layer phosphorene by liquid exfoliation of black phosphorus, Chem. Commun. 50 (2014) 13338–13341, doi:10.1039/c4cc05752j.

[32] Z. Luo, Y. Li, M. Zhong, Y. Huang, X. Wan, J. Peng, J. Weng, Nonlinear optical absorption of few-layer molybdenum diselenide ($MoSe_2$) for passively mode-locked soliton fiber laser, Photonics Res. 3 (2015) A79, doi:10.1364/prj.3.000a79.

[33] Y. Hernandez, V. Nicolosi, M. Lotya, F.M. Blighe, Z. Sun, S. De, I.T. McGovern, B. Holland, M. Byrne, Y.K. Gun'ko, J.J. Boland, P. Niraj, G. Duesberg, S. Krishnamurthy, R. Goodhue, J. Hutchison, V. Scardaci, A.C. Ferrari, J.N. Coleman, High-yield production of graphene by liquid-phase exfoliation of graphite, Nat. Nanotechnol. 3 (2008) 563–568, doi:10.1038/nnano.2008.215.

[34] P. Yasaei, B. Kumar, T. Foroozan, C. Wang, M. Asadi, D. Tuschel, J.E. Indacochea, R.F. Klie, A. Salehi-Khojin, High-quality black phosphorus atomic layers by liquid-phase exfoliation, Adv. Mater. 27 (2015) 1887–1892, doi:10.1002/adma.201405150.

[35] M. Lotya, A. Rakovich, J.F. Donegan, J.N. Coleman, Measuring the lateral size of liquid-exfoliated nanosheets with dynamic light scattering, Nanotechnology 24 (2013) 265703, doi:10.1088/0957-4484/24/26/265703.

[36] B. Adilbekova, Y. Lin, E. Yengel, H. Faber, G. Harrison, Y. Firdaus, A. El-Labban, D.H. Anjum, V. Tung, T.D. Anthopoulos, Liquid phase exfoliation of MoS_2 and WS_2 in aqueous ammonia and their application in highly efficient organic solar cells, J. Mater. Chem. C 8 (2020) 5259–5264, doi:10.1039/d0tc00659a.

[37] T.K. Mukhopadhyay, A. Datta, Deciphering the role of solvents in the liquid phase exfoliation of hexagonal boron nitride: a molecular dynamics simulation study, J. Phys. Chem. C 121 (2017) 811–822, doi:10.1021/acs.jpcc.6b09446.

[38] S.S. Chhatre, J.O. Guardado, B.M. Moore, T.S. Haddad, J.M. Mabry, Fluoroalkylated silicon-containing surfaces-estimation of solid surface energy, ACS Appl. Mater. Interfaces 2 (2010) 3544–3554.

[39] Y.S. Singh, S.B. Singh, R. Priya, J. Rajiv, G. Ayush, Surface tension measurement of normal human blood samples by pendant Surface tension measurement of normal human blood samples by pendant drop method Siddharth Singh Yadav, Basant Singh Sikarwar, Priya Ranjan, Rajiv, J. Med. Eng. Technol. 44 (2020) 227–236, doi:10.1080/03091902.2020.1770348.

[40] Z. Gholamvand, D. McAteer, C. Backes, N. McEvoy, A. Harvey, N.C. Berner, D. Hanlon, C. Bradley, I. Godwin, A. Rovetta, M.E.G. Lyons, G.S. Duesberg, J.N. Coleman, Comparison of liquid exfoliated transition metal dichalcogenides reveals $MoSe_2$ to be the most effective hydrogen evolution catalyst, Nanoscale 8 (2016) 5737–5749, doi:10.1039/c5nr08553e.

[41] J. Gao, W. Jie, Y. Yuan, T. Wang, G. Zha, J. Tong, Dependence of film texture on substrate and growth conditions for CdTe films deposited by close-spaced sublimation, J. Vac. Sci. Technol. A 29 (2011) 051507 Vacuum Surfaces Film., doi:10.1116/1.3610177.

[42] C. Prabukumar, M.M.J. Sadiq, D.K. Bhat, K.U. Bhat, Effect of solvent on the morphology of MoS_2 nanosheets prepared by ultrasonication-assisted exfoliation, AIP Conf. Proc. 1943 (2018) 020084, doi:10.1063/1.5029660.

[43] P. Ge, H. Hou, C.E. Banks, C.W. Foster, S. Li, Y. Zhang, J. He, C. Zhang, X. Ji, Binding $MoSe_2$ with carbon constrained in carbonous nanosphere towards high-capacity and ultrafast Li/Na-ion storage, Energy Storage Mater. 12 (2018) 310–323, doi:10.1016/j.ensm.2018.02.012.
[44] C. Dai, Z. Zhou, C. Tian, Y. Li, C. Yang, X. Gao, X. Tian, Large-scale synthesis of graphene-like $MoSe_2$ nanosheets for efficient hydrogen evolution reaction, J. Phys. Chem. C 121 (2017) 1974–1981, doi:10.1021/acs.jpcc.6b11423.
[45] H. Mittal, M. Khanuja, Interfacial charge carrier dynamics of the $MoSe_2$-conducting polymer ($MoSe_2$-PANI) heterojunction, Mater. Today Proc. 28 (2020) 314–316.
[46] S.K. Sahu, P. Choudhury, K. Behera, T. Bisoyi, Oxygen Bridged Bimetallic [Cu-O-Se] catalyst for sonogashira cross-coupling, New J. Chem. 46 (2022) 1650–1657.
[47] S.K. Sahoo, A. Mallik, Simple, fast and cost-effective electrochemical synthesis of few layer graphene nanosheets, Nano 10 (2015) 1550019, doi:10.1142/S1793292015500198.
[48] M.A. Diasio, Rheological and colloidal approaches to characterizing and producing dispersions for advanced manufacturing, Doctoral Dissertation, University of Virginia, 2019, doi:10.18130/v3-q4xs-5s35.
[49] C. Backes, B.M. Szydłowska, A. Harvey, S. Yuan, V. Vega-Mayoral, B.R. Davies, P.L. Zhao, D. Hanlon, E.J.G. Santos, M.I. Katsnelson, W.J. Blau, C. Gadermaier, J.N. Coleman, Production of highly monolayer enriched dispersions of liquid-exfoliated nanosheets by liquid cascade centrifugation, ACS Nano 10 (2016) 1589–1601, doi:10.1021/acsnano.5b07228.
[50] N. Dong, Y. Li, Y. Feng, S. Zhang, X. Zhang, C. Chang, J. Fan, L. Zhang, J. Wang, Optical limiting and theoretical modelling of layered transition metal dichalcogenide nanosheets, Sci. Rep. 5 (2015) 14646, doi:10.1038/srep14646.
[51] R. Sharma, A. Dawar, S. Ojha, R. Laishram, V.G. Sathe, R. Srivastava, O.P. Sinha, A thrifty liquid-phase exfoliation (LPE) of $MoSe_2$ and WSe_2 nanosheets as channel materials for FET application, J. Electron. Mater. 52 (2023) 2819–2830, doi:10.1007/s11664-023-10245-9.
[52] S. Samikannu, S. Sivaraj, Dissipative soliton generation in an all-normal dispersion ytterbium-doped fiber laser using few-layer molybdenum diselenide as a saturable absorber, Opt. Eng. 55 (2016) 081311, doi:10.1117/1.oe.55.8.081311.
[53] E. Varrla, C. Backes, K.R. Paton, A. Harvey, Z. Gholamvand, J. McCauley, J.N. Coleman, Large-scale production of size-controlled MoS_2 nanosheets by shear exfoliation, Chem. Mater. 27 (2015) 1129–1139, doi:10.1021/cm5044864.
[54] C. Backes, R.J. Smith, N. McEvoy, N.C. Berner, D. McCloskey, H.C. Nerl, A. O'Neill, P.J. King, T. Higgins, D. Hanlon, N. Scheuschner, J. Maultzsch, L. Houben, G.S. Duesberg, J.F. Donegan, V. Nicolosi, J.N. Coleman, Edge and confinement effects allow *in situ* measurement of size and thickness of liquid-exfoliated nanosheets, Nat. Commun. 5 (2014) 4576, doi:10.1038/ncomms5576.
[55] C. Backes, T.M. Higgins, A. Kelly, C. Boland, A. Harvey, D. Hanlon, J.N. Coleman, Guidelines for exfoliation, characterization and processing of layered materials produced by liquid exfoliation, Chem. Mater. 29 (2017) 243–255, doi:10.1021/acs.chemmater.6b03335.
[56] J.K. Ellis, M.J. Lucero, G.E. Scuseria, The indirect to direct band gap transition in multilayered MoS_2 as predicted by screened hybrid density functional theory, Appl. Phys. Lett. 99 (2011) 261908, doi:10.1063/1.3672219.
[57] I.G. Lezama, A. Ubaldini, M. Longobardi, E. Giannini, C. Renner, A.B. Kuzmenko, A.F. Morpurgo, Surface transport and band gap structure of exfoliated 2H-$MoTe_2$ crystals, 2D Mater. 1 (2014) 021002, doi:10.1088/2053-1583/1/2/021002.